

Magmatic ignitor kick-starts subduction initiation

Jianfeng Yang¹, Baolu Sun², Chang Zhang¹, and Liang Zhao²

¹Institute of Geology and Geophysics, Chinese Academy of Sciences

²State Key Laboratory of Lithospheric Evolution, Institute of Geology and Geophysics, Chinese Academy of Sciences

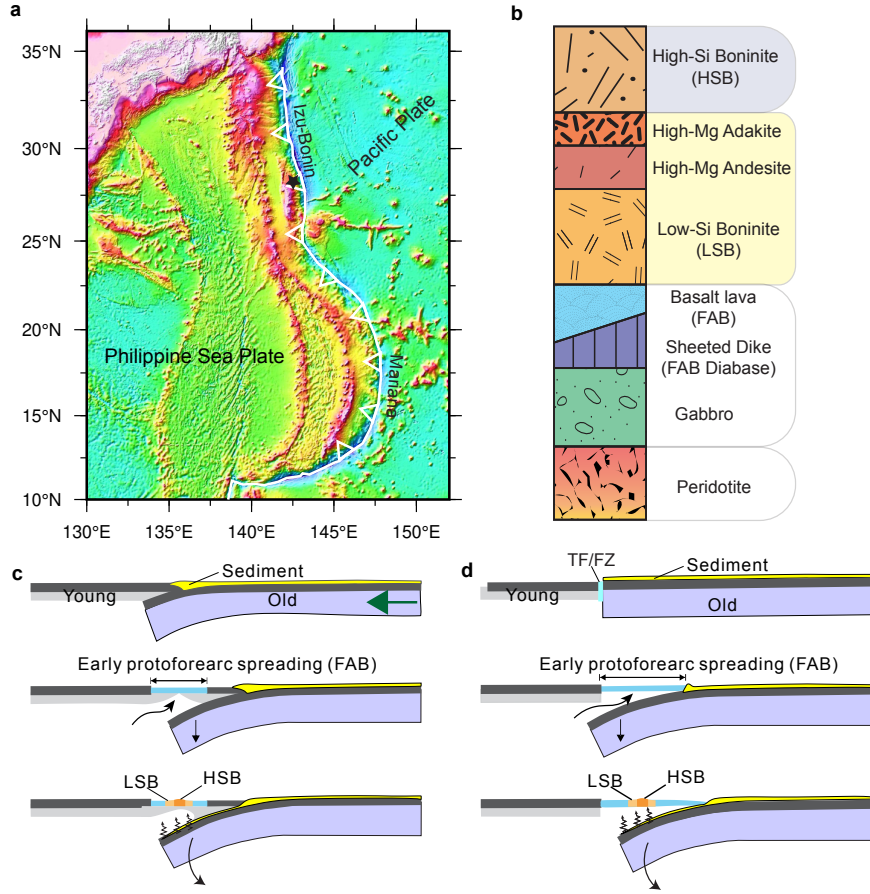
November 22, 2022

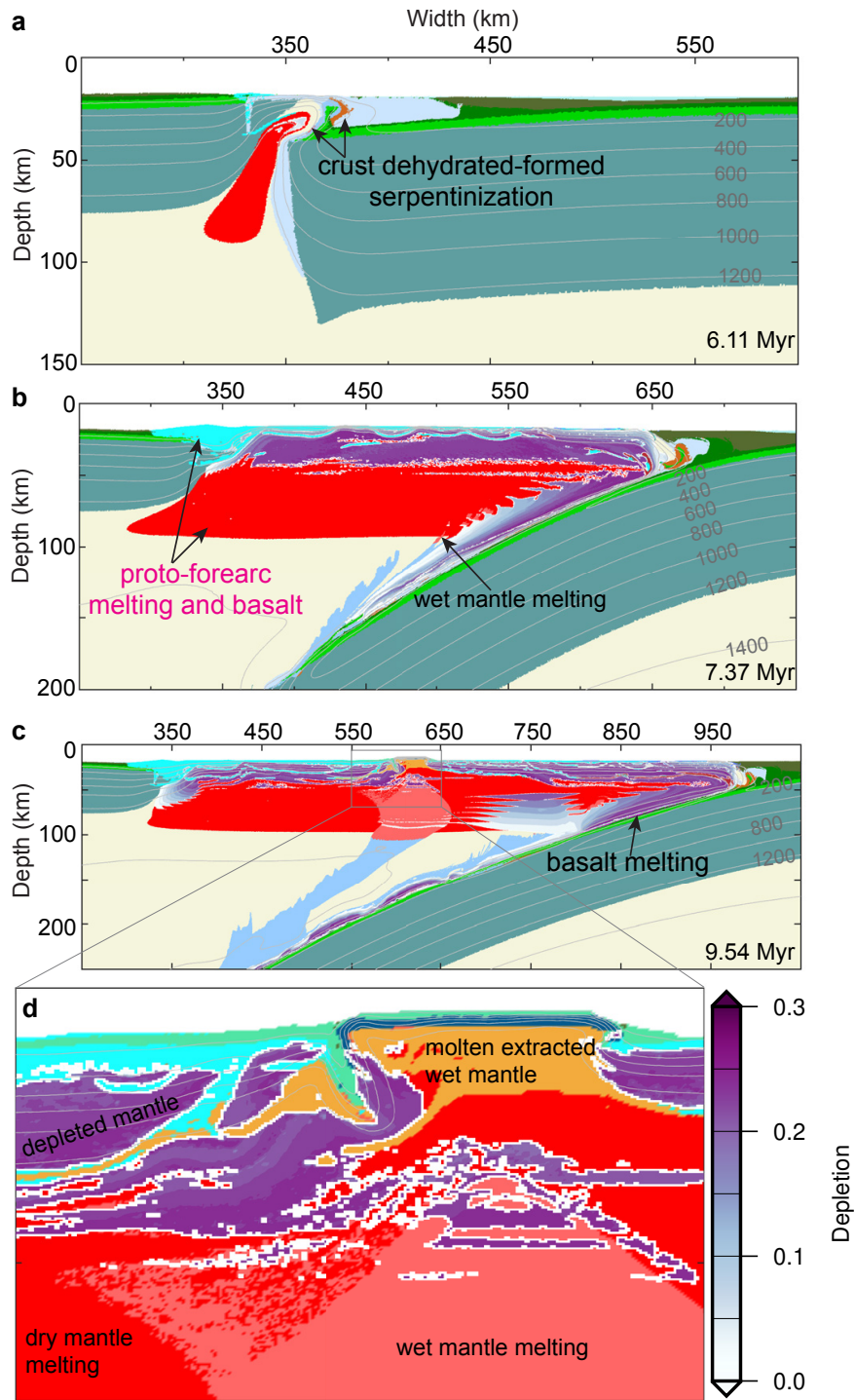
Abstract

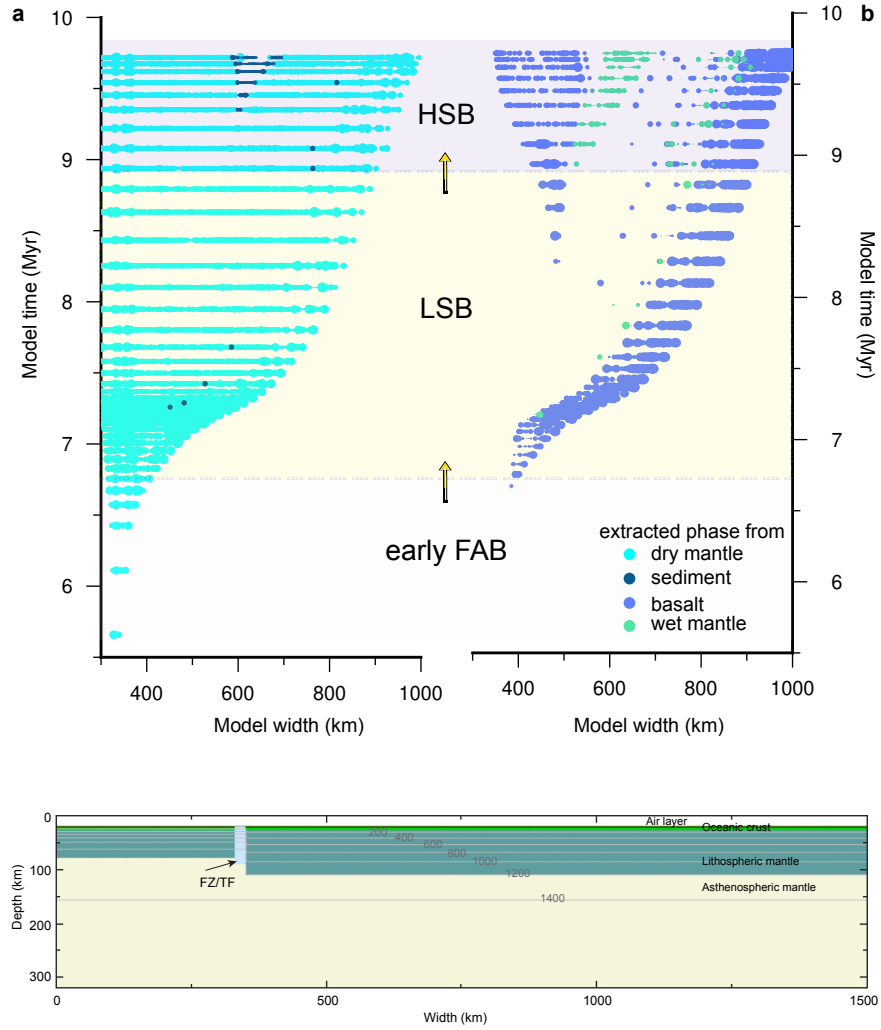
Subduction is fundamental for maintaining plate tectonics. Magmatic record of subduction initiation offers pivotal clues for understanding the nucleation and propagation of a new subduction zone. However, how subduction is elicited to induce the first-order magmatic observations is yet to be understood. Here, using numerical models, we demonstrate that magmatic ignitor of mantle melting triggered-upwelling along wide and weak fracture zones renders lithospheric mantle sinking and subduction initiation. Progressive decompression melting is sequentially followed by melting of oceanic crust, hydrated and depleted mantle, and sediment of the retreating slab, respectively. This scenario is compatible with the in-situ observations of petrogenesis in the western Pacific, which also explains the enigmatic deferred sediment involvement in the early magmatism. Our self-consistent model indicates that a continuous magmatic ignitor beneath a transform fault resulting in subduction initiation could be a prevalent process in Earth's evolution.

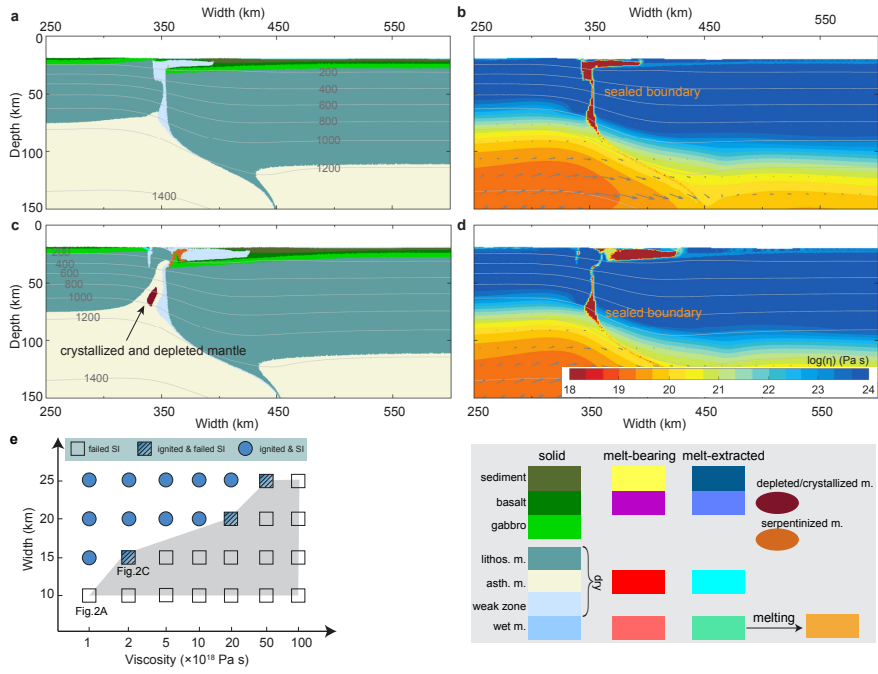
Hosted file

essoar.10511755.1.docx available at <https://authorea.com/users/536431/articles/599074-magmatic-ignitor-kick-starts-subduction-initiation>









Magmatic ignitor kick-starts subduction initiation

Jianfeng Yang^{1,*}, Baolu Sun¹, Chang Zhang¹, Liang Zhao¹

¹ *State Key Laboratory of Lithospheric Evolution, Institute of Geology and Geophysics, Chinese Academy of Sciences, 100029 Beijing, China*

Corresponding author: J.Yang (yangjf@mail.iggcas.ac.cn)

Key points

- Subduction initiation is triggered by the magmatic ignitor
- First-order magmatic records can be reproduced by petrological-thermomechanical models
- Subduction initiation in intra-ocean could be prevalent in geologic time

Abstract

Subduction is fundamental for maintaining plate tectonics. Magmatic record of subduction initiation offers pivotal clues for understanding the nucleation and propagation of a new subduction zone. However, how subduction is elicited to induce the first-order magmatic observations is yet to be understood. Here, using numerical models, we demonstrate that magmatic ignitor of mantle melting triggered-upwelling along wide and weak fracture zones renders lithospheric mantle sinking and subduction initiation. Progressive decompression melting is sequentially followed by melting of oceanic crust, hydrated and depleted mantle, and sediment of the retreating slab, respectively. This scenario is compatible with the in-situ observations of petrogenesis in the western Pacific, which also explains the enigmatic deferred sediment involvement in the early magmatism. Our self-consistent model indicates that a continuous magmatic ignitor beneath a transform fault resulting in subduction initiation could be a prevalent process in Earth's evolution.

Plain language

Subduction initiation (SI) is a key process through geological time in terms of plate tectonics. However, SI is a destructive process that leaves very sporadic geologic records. Thus, how subduction is initiated remains an outstanding question and hotly debated. Izu-Bonin-Mariana is an ideal location to study SI because a comprehensive magmatic record has been preserved during SI, which provides crucial hints on the conditions and dynamics of SI. In this study, we use petrological-thermomechanical numerical models, to reproduce the first-order of magmatic observations. Our models show that a starting fire by mantle melting beneath the fracture zones/transform fault can trigger subduction initiation. The resulting magmatism can be compatible with the petrogenesis in the Izu-Bonin-Mariana. We further demonstrate that a wide and weak transform fault to initiate a new subduction zone could frequently occur in the intra-ocean.

Introduction

Subduction is a fundamental process in which the negatively buoyant oceanic plate provides the principal driving force for plate tectonics. Initiation of new subduction zones is a crucial process for Earth’s evolution. However, the mechanisms of how and where a new subduction zone is established remain controversial (Stern and Gerya, 2018; Cramer et al., 2020). Subduction initiation (SI) is difficult to spontaneously occur at the present-day passive margin where the oceanic plate is old, and plate sinking is resisted by substantial bending and shear forces (Nikolaeva et al., 2010; Zhong and Li, 2019). The majority of the Cenozoic subduction zones in the western Pacific, on the other hand, are of intra-oceanic origin, implying more favorable conditions for SI (Gurnis et al., 2004). Oceanic transform faults widely distributed in the ocean are plate boundaries that separate rigid plates. They leave spectacular morphological scars on the seafloor called fracture zones. These fracture zones are weak areas that are likely to have a significant impact on the SI. Indeed, a statistical compilation of SI over the last 100 Ma indicates that SI is tightly linked to pre-existing weak zones (Cramer et al., 2020).

The classical “spontaneous SI” suggests a negatively buoyant and old oceanic plate founder along a transform fault or fracture zones (Fig. 1, Stern and Bloomer, 1992; Whattam and Stern, 2011; Leng et al., 2015; Zhou et al., 2018; Arcay et al., 2020). An oceanic plate, however, cannot subduct spontaneously due to significant resistive forces until subduction inception or stable subduction is attained (Cramer et al., 2020). This indicates that subduction inception must be elicited by an external trigger, which can be either horizontal or vertical. Numerical models indeed suggest either horizontal convergence (Hall et al., 2003; Gurnis et al., 2004; Lu et al., 2015; Sun et al., 2021; Almeida et al., 2022) or significant vertical pull (Maunder et al., 2020) is required before lithospheric subduction occurs.

SI is a destructive and ephemeral process that leaves sporadic and disputed evidence in its wake. However, the abundant magmatic records during subduction initiation have been well-established thanks to the IODP expeditions. A comprehensive magmatic record in Izu-Bonin-Mariana (IBM) provides crucial hints on the dynamics of SI. The magmatic sequence of forearc basalts (FAB), low-silica boninites (LSB), high-silica boninites (HSB), tholeiites, and calc-alkaline (andesitic) are the archetypal magma types (Arculus et al., 2015; Fig. 1). The product of decompression mantle melting characterized by MORB-like basalts is termed FAB (Reagan et al., 2010). The latter involvement of slab-derived melts to the refractory mantle wedge is key to the formation of boninites. Geochemical records suggest that sediments involvement postdates the occurrence of FAB and boninites. The removal of sediment from the slab prior to plate foundering suggests a necessary horizontal convergence between the upper plate and the future lower plate (Gurnis et al., 2004; Hall et al., 2003; Li et al., 2019). The horizontal force must therefore take precedence over the vertical force. However, numerical models demonstrate that a horizontally forced SI cannot yield FAB (Maunder et al., 2020). As a result, a vertical force is needed. To circumvent the difficulty of SI, previous numerical models postulated a large vertical pull

force which is not straightforward to explain its provenance. Here we propose a new mechanism that a magmatic ignitor along the fracture zones that elicits upward mantle flow and subsequent dense plate sinking to initiate subduction.

Methods

The 2D petrological-thermomechanical numerical code I2VIS (Gerya and Yuen, 2003) used in this study is based on a finite difference method employing the marker-in-cell technique on a staggered grid. It solves mass, momentum, and energy conservation equations (eq. 1-3) on the Eulerian grid and interpolates physical properties back to the markers for advection accordingly.

$$\frac{\partial v_i}{\partial x_i} = 0 \quad (1)$$

$$-\frac{\partial P}{\partial x_i} + \frac{\partial}{\partial x_j}(\eta(\frac{\partial v_i}{\partial x_j} + \frac{\partial v_j}{\partial x_i})) + \rho g_i = 0 \quad (2)$$

$$\rho c_p \left(\frac{\partial T}{\partial t} + v_i \frac{\partial T}{\partial x_i} \right) = \frac{\partial}{\partial x_i} \left(k \frac{\partial T}{\partial x_i} \right) + H_r + H_s + H_a \quad (3)$$

where v_i is velocity, x_i coordinate, P dynamic pressure, ρ density, g gravity acceleration, c_p heat capacity, T temperature, k thermal conductivity, H_r radioactive heating, shear heating $H_s = \tau_{ij} \dot{\epsilon}_{ij}$ and adiabatic heating $H_a = T \alpha \frac{DP}{Dt}$. The latent heat is implicitly considered by computing the effective thermal expansion and heat capacity (Gerya and Yuen, 2003).

The initial model setup is built upon the subduction initiation of the Izu-Bonin-Mariana (IBM) subduction system. The model is 1500×320 km (resolved with 1001×321 nodes), with a young (10 Myr old) and an old oceanic plate (50 Myr old) on the left and right sides and a weak zone in between, respectively. The model uses a free-slip mechanical boundary condition for all boundaries except the permeable lower boundary. While the top boundary implements a 20-km-thick ‘sticky-air’ with low viscosity (10^{18} Pa s) to mimic a free surface (Schmeling et al., 2008; Cramer et al., 2012). The initial thermal structure is defined by a half-space cooling model for the oceanic plates and an adiabatic thermal gradient of 0.5 K/km for the underlying asthenosphere. The top and bottom boundaries have isotherm temperatures of 273 K and 1750 K, respectively. The side boundaries are insulative with zero heat flux.

The rheology of rocks is assumed to be visco-plastic, which combines ductile (dislocation and diffusion) and brittle (Drucker-Prager) deformation. The effective ductile viscosity is given by the harmonic average of dislocation and diffusion creep below:

$$\eta_{ductile0} = \left(\frac{1}{\eta_{disl}} + \frac{1}{\eta_{diff}} \right)^{-1} \quad (4)$$

$$\eta_{diff} = \frac{1}{2} A_d \tau_{cr}^{n-1} \exp\left(\frac{E+PV}{RT}\right) \quad (5)$$

$$\eta_{disl} = \frac{1}{2} A_d^{1/n} \dot{\epsilon}_{II}^{1/n-1} \exp\left(\frac{E+PV}{nRT}\right) \quad (6)$$

where η_{diff} , η_{disl} are the viscosity of diffusion and dislocation creep, respectively. τ_{cr} (1 MPa) is the assumed diffusion-dislocation transition stress, A_d , E , V ,

n are viscosity prefactor, activation energy, activation volume, and stress exponent, respectively (see the physical parameters in Supplementary Table S1). For the hydrated and/or partially molten and/or depleted rocks, viscosity can be reduced (by hydration and melting) or strengthened (by devolatilization after melt extraction) and is expressed as (Hirth and Kohlstedt, 2003; Yang and Faccenda, 2020; Capitanio et al., 2020),

$$\eta_{\text{ductile}} = \eta_{\text{ductile}0} \left(\frac{C_w}{C_{w0}}\right)^{-\frac{r}{n}} \exp(-\alpha\phi/n) \left(1 - \frac{\Phi_{\text{ext}}}{\Phi_{\text{max}}}\right)^{-2.5} \quad (7)$$

where C_w , C_{w0} are water content and reference water content (0.01 wt%), respectively. ϕ , Φ_{ext} , Φ_{max} are melt fraction, extracted melt fraction, and maximum extracted melt fraction (0.8 is used), respectively, $\alpha = 28$ is a constant (Hirth and Kohlstedt, 2003).

Rocks fail brittlely/plastically when the second invariant stress exceeds the yield stress,

$$\eta_{\text{ductile}} \leq \frac{C + \mu P}{2\dot{\epsilon}_{\text{II}}} \quad (8)$$

where C , μ , $\dot{\epsilon}_{\text{II}}$ are cohesion, internal friction coefficient, and second invariant of strain rate tensor, respectively.

The solid-solid phase changes are incorporated in the density and enthalpy lookup tables obtained from PERPLE_X (Connolly, 2005). Mantle melting uses the parameterization of Katz et al. (2003), and melting of the crust and sediment uses a linear relationship of the solidus and liquidus,

$$\phi_0 = \frac{T - T_s}{T_l - T_s} \quad (9)$$

where T_s , T_l are solidus and liquidus, respectively.

The melt extraction approach follows previous studies (Yang et al., 2020; Yang and Faccenda, 2020), and it is worth noting that the melt fraction has to take into account the extracted melt. Thus, the melt fraction at each time step is

$$\phi = \phi_0 - \Phi_{\text{ext}} \quad (10)$$

Results

Failed or incompatible subduction initiation

We designed a self-consistent intra-oceanic model setup with a specific breadth of the weak zone (to mimic the transform fault/fracture zones) inserted between a young and an old oceanic plate (Fig. 2). The relatively buoyant weak zone flows upward, while either a too thin or too strong zone cannot induce asthenospheric upwelling or partial melting. If no external forces are applied, or persistent upwelling asthenosphere is absent, the plate boundary is swiftly sealed (Fig. 3). A relatively wider weak zone, on the other hand, causes rapid upwelling and decompression melting at first. However, the upward flow is still inadequate to trigger continuous mantle melting, and the shallow mantle cools and strengthens again (Fig. 3). Thus, neither possibility succeeds in establishing a new subduction zone without sustaining mantle melting.

We test a horizontally forced subduction initiation model by imposing a pushing on the old plate (Fig. S1). Early forearc basalt is absent, and slab components such as sediment/basalt melting and flux mantle melting occur before dry decompression melting. This is inconsistent with the magmatic records in IBM (Reagan et al., 2010; Maunder et al., 2020); we thus deduce that SI in IBM may not be dominated by horizontal force.

Subduction initiation triggered by decompression melting and subsequent petrogenesis

For a rheologically weaker and wider weak zone, decompression melting forms continuously, and the partially molten mantle intrudes upward quickly due to its low viscosity and density (Fig. 3E, S2). The young and old plates are completely decoupled, and the hot upwelling spreads laterally towards the old plate, accompanied by the old plate foundering simultaneously. Progressive adiabatic decompression melting occurs at the hot void where the downgoing slab leaves. The slab tip directly contacts the hot asthenosphere, which may result in a high-temperature metamorphic sole (Zhou and Wada, 2021). After ~ 0.4 Myr of the earliest decompression melting, the gabbro at the slab tip starts to dehydrate when quickly heated to ~ 700 °C. In addition, a portion of the uppermost asthenosphere is cooled down to serpentine stability. Subsequent crustal dehydration further promotes decoupling between the subducting slab and the overriding plate. The buoyant and weak sediments are driven away from the slab tip by the retreating hot mantle, which significantly delays its involvement in the early magmatism. The partially molten asthenosphere is extracted to form the early FAB at the surface (Fig. 4). There is essentially minimal contribution of the subducting slab to develop the early FABs (Fig. 5). The non-extractable melt creates a very weak mantle wedge, and continuing fertile asthenosphere from the west side replenishes the wedge to form new FABs. The trench retreats quickly, and the hot mantle heats the basaltic layer, causing it to partially melt. The mantle wedge is severely depleted (~ 15 - 25% of depletion), and the ocean crust starts to dehydrate substantially when the slab reaches ~ 150 - 200 km. The addition of water and sediment into the depleted harzburgitic residue results in further melting. This is in line with the proposed formation of high-silica boninites.

Discussion

Seismic observations show low velocity down to ~ 16 km beneath the transform faults, suggesting that seawater circulates along fractures to hydrate the mantle (Batista et al., 2017), resulting in significant lower strength and lower density (Gerya et al., 2016; Hensen et al., 2019; Wolfson-Schwehr et al., 2019). Our model shows that a wider, lighter, and weaker fracture zone promotes the occurrence of SI (Fig. 3). Geophysical and geological observations show that the breadth of the transform faults is generally narrow to 1-10 km, which is insufficient for SI, while only a few regions are up to 20-40 km (Wolfson-Schwehr et al., 2019). Nevertheless, the width of the damage zone increases by stress concentration of repeating earthquakes on ridge-transform fault (Wolfson-Schwehr

et al., 2014); or by plate rotation-induced “leaky transform fault” (Casey and Dewey, 1984; Pockalny et al., 1996). There is no geologic track of the stress state of the transform faults that predates the SI occurrence. However, the Pacific Plate indeed underwent clockwise rotation at ~50 Ma, which is nearly contemporarily with the SI of IBM (Wu et al., 2016; Reagan et al., 2019). The rotation of the Pacific Plate, likely resulting in the widening of the fracture zone, provides a superb condition for the magmatic ignitor and subsequent SI, as our model shows.

The early FAB is a crucial indicator of SI. The asthenosphere experiences 15-25% melt extraction to be a very depleted mantle wedge consistent with the geochemical modeling of 7-23% melting of a mantle source to generate the low-Ti-K FAB and boninites (Shervais et al., 2019; Li et al., 2021; Leng et al., 2012). It has been suggested that the early FAB resulted from dry decompression melting in the absence of slab-derived fluids. We further test two models with a dry gabbroic and a dry basaltic layer, respectively (Fig. S3). The model results demonstrate that basalt dehydration renders shallow mantle serpentinization, while the limited dehydration cannot lubricate the plate interface before upwelling cools down. On the contrary, the dehydration of gabbro results in slightly wet melting that decouples two plates, and subduction continues. It is worth noting that the presence of fluid/melt from the slab is minute during subduction inception, yet its effect on lubricating the plate interface cannot be disregarded (Dymkova and Gerya, 2013; Agard et al., 2020). The drilled FAB from IODP Expedition 352 shows that FAB are also relatively enriched in fluid-mobile elements with high H₂O/Ce and Cl/K ratios compared to normal MORB (Coulthard Jr et al., 2020), likely results from minor contribution from the early ocean crust dehydration. The dredged adakitic magmatism in the Bonin forearc, having extremely high Sr and low Y contents, are coeval or slightly postdate the boninites (Li et al., 2013). Isotopic fingerprints provide robust evidence that slab melts of Pacific altered basaltic crust are involved in LSB genesis (Li et al., 2019). Our numerical models exhibit the pervasive melting of the dry mantle accompanied by basaltic melting during fast trench retreat and heat up of the slab surface. Therefore, the LSB may result from in mixing of shallow dry mantle melting and ocean crust melting (Fig. 5). The addition of slab-derived fluids into the depleted mantle residue results in further melting, while sediments were additionally involved in HSB genesis at a later stage.

The ongoing SI of Puysegur has been attributed to horizontally forced subduction with upper plate compression during subduction inception (Shuck et al., 2022). No FAB are reported in Puysegur, which implies a vertical force dominance for the occurrence of FAB in IBM SI. Our model shows that a magmatic ignitor triggering continuous asthenospheric upwelling beneath fracture zones and lateral propagation to initiate a new subduction zone that exhibits resembant petrogenesis sequence could be a prevalent process for SI.

References

- Agard, P., C. Prigent, M. Soret, B. Dubacq, S. Guillot, and D. Deldicque (2020), Slabification: Mechanisms controlling subduction development and viscous coupling, *Earth Sci. Rev.*, 208, 103259, <https://doi.org/10.1016/j.earscirev.2020.103259>.
- Almeida, J., N. Riel, F. M. Rosas, J. C. Duarte, and B. Kaus (2022), Self-replicating subduction zone initiation by polarity reversal, *Communications Earth & Environment*, 3(1), 55, doi:10.1038/s43247-022-00380-2.
- Arcay, D., S. Lallemand, S. Abecassis, and F. Garel (2020), Can subduction initiation at a transform fault be spontaneous?, *Solid Earth*, 11(1), 37-62. <https://doi.org/10.5194/se-11-37-2020>.
- Arculus, R. J., O. Ishizuka, K. A. Bogus, M. Gurnis, R. Hickey-Vargas, M. H. Aljahdali, A. N. Bandini-Maeder, A. P. Barth, P. A. Brandl, and L. Drab (2015), A record of spontaneous subduction initiation in the Izu-Bonin-Mariana arc, *Nat. Geosci.*, 8(9), 728. <https://doi.org/10.1038/ngeo2515>.
- Batista, L., C. Hübscher, P. Terrinha, L. Matias, A. Afilhado, and T. Lüdmann (2017), Crustal structure of the Eurasia–Africa plate boundary across the Gloria fault, north Atlantic ocean, *Geophys. J. Int.*, 209(2), 713-729. <https://doi.org/10.1093/gji/ggx050>.
- Capitania, F. A., O. Nebel, and P. A. Cawood (2020), Thermochemical lithosphere differentiation and the origin of cratonic mantle, *Nature*, 588(7836), 89-94, doi:10.1038/s41586-020-2976-3.
- Casey, J., and J. F. Dewey (1984), Initiation of subduction zones along transform and accreting plate boundaries, triple-junction evolution, and forearc spreading centres—implications for ophiolitic geology and obduction, Geological Society, London, Special Publications, 13(1), 269-290.
- Connolly, J. (2005), Computation of phase equilibria by linear programming: a tool for geodynamic modeling and its application to subduction zone decarbonation, *Earth Planet. Sci. Lett.*, 236(1), 524-541, <https://doi.org/10.1016/j.epsl.2005.04.033>.
- Coulthard Jr, D. A., M. K. Reagan, K. Shimizu, I. N. Bindeman, M. Brounce, R. R. Almeev, J. Ryan, T. Chapman, J. Shervais, and J. A. Pearce (2021), Magma source evolution following subduction initiation: Evidence from the element concentrations, stable isotope ratios, and water contents of volcanic glasses from the Bonin forearc (IODP expedition 352), *Geochem. Geophys. Geosyst.*, 22(1), e2020GC009054.
- Crameri, F., et al. (2020), A transdisciplinary and community-driven database to unravel subduction zone initiation, *Nat. Commun.*, 11(1), 3750, doi:10.1038/s41467-020-17522-9.
- Crameri, F., H. Schmeling, G. Golabek, T. Duretz, R. Orendt, S. Buitter, D. May, B. Kaus, T. Gerya, and P. Tackley (2012), A comparison of numerical surface topography calculations in geodynamic modelling: an evaluation of the ‘sticky

- air'method, *Geophys. J. Int.*, 189(1), 38-54. <https://doi.org/10.1111/j.1365-246X.2012.05388.x>.
- Dymkova, D., and T. Gerya (2013), Porous fluid flow enables oceanic subduction initiation on Earth, *Geophys. Res. Lett.*, 40(21), 5671-5676, Doi 10.1002/2013gl057798.
- Gerya, T. V. (2016), Origin, evolution, seismicity, and models of oceanic and continental transform boundaries, *Plate Boundaries and Natural Hazards*, AGU Geophysical Monograph Series, 219, 39-76.
- Gerya, T. V., and D. A. Yuen (2003), Characteristics-based marker-in-cell method with conservative finite-differences schemes for modeling geological flows with strongly variable transport properties, *Phys. Earth Planet. Inter.*, 140(4), 293-318, <https://doi.org/10.1016/j.pepi.2003.09.006>.
- Gurnis, M., C. Hall, and L. Lavier (2004), Evolving force balance during incipient subduction, *Geochem. Geophys. Geosyst.*, 5(7), Q07001, doi:10.1029/2003GC000681.
- Hall, C. E., M. Gurnis, M. Sdrolias, L. L. Lavier, and R. D. Müller (2003), Catastrophic initiation of subduction following forced convergence across fracture zones, *Earth Planet. Sci. Lett.*, 212(1), 15-30. [https://doi.org/10.1016/S0012-821X\(03\)00242-5](https://doi.org/10.1016/S0012-821X(03)00242-5).
- Hensen, C., J. C. Duarte, P. Vannucchi, A. Mazzini, M. A. Lever, P. Terrinha, L. Géli, P. Henry, H. Villinger, and J. Morgan (2019), Marine transform faults and fracture zones: a joint perspective integrating seismicity, fluid flow and life, *Front. Earth Sci.*, 39. <https://doi.org/10.3389/feart.2019.00039>.
- Hirth, G., and D. Kohlstedt (2003), Rheology of the upper mantle and the mantle wedge: A view from the experimentalists, *Geophysical Monograph Series*, 138, 83-105.
- Ishizuka, O., R. N. Taylor, S. Umino, and K. Kanayama (2020), Geochemical evolution of arc and slab following subduction initiation: a record from the Bonin Islands, Japan, *J. Petrol.*, 61(5), ega050. <https://doi.org/10.1093/petrology/egaa050>.
- Katz, R. F., M. Spiegelman, and C. H. Langmuir (2003), A new parameterization of hydrous mantle melting, *Geochem. Geophys. Geosyst.*, 4(9), 1073, doi:10.1029/2002GC000433.
- Leng, W., and M. Gurnis (2015), Subduction initiation at relic arcs, *Geophys. Res. Lett.*, 42(17), 7014-7021. <https://doi.org/10.1002/2015GL064985>.
- Leng, W., M. Gurnis, and P. Asimow (2012), From basalts to boninites: The geodynamics of volcanic expression during induced subduction initiation, *Lithosphere*, 4(6), 511-523. <https://doi.org/10.1130/L215.1>.
- Li, H., et al. (2021), Basalt derived from highly refractory mantle sources during early Izu-Bonin-Mariana arc development, *Nat. Commun.*, 12(1), 1723, doi:10.1038/s41467-021-21980-0.

- Li, H.-Y., R. N. Taylor, J. Prytulak, M. Kirchenbaur, J. W. Shervais, J. G. Ryan, M. Godard, M. K. Reagan, and J. A. Pearce (2019), Radiogenic isotopes document the start of subduction in the Western Pacific, *Earth Planet. Sci. Lett.*, 518, 197-210. <https://doi.org/10.1016/j.epsl.2019.04.041>.
- Li, Y.-B., J.-I. Kimura, S. Machida, T. Ishii, A. Ishiwatari, S. Maruyama, H.-N. Qiu, T. Ishikawa, Y. Kato, and S. Haraguchi (2013), High-Mg adakite and low-Ca boninite from a Bonin fore-arc seamount: implications for the reaction between slab melts and depleted mantle, *J. Petrol.*, 54(6), 1149-1175. <https://doi.org/10.1093/petrology/egt008>.
- Lu, G., B. J. Kaus, L. Zhao, and T. Zheng (2015), Self-consistent subduction initiation induced by mantle flow, *Terra Nova*, 27(2), 130-138. <https://doi.org/10.1111/ter.12140>.
- Maunder, B., J. Prytulak, S. Goes, and M. Reagan (2020), Rapid subduction initiation and magmatism in the Western Pacific driven by internal vertical forces, *Nat. Commun.*, 11(1), 1874, doi:10.1038/s41467-020-15737-4.
- Nikolaeva, K., T. Gerya, and F. Marques (2010), Subduction initiation at passive margins: numerical modeling, *J. Geophys. Res.: Solid Earth (1978–2012)*, 115(B3). <https://doi.org/10.1029/2009JB006549>.
- Pockalny, R. A., P. Gente, and R. Buck (1996), Oceanic transverse ridges: A flexural response to fracture-zone-normal extension, *Geology*, 24(1), 71-74.
- Reagan, M. K., D. E. Heaton, M. D. Schmitz, J. A. Pearce, J. W. Shervais, and A. A. Koppers (2019), Forearc ages reveal extensive short-lived and rapid seafloor spreading following subduction initiation, *Earth Planet. Sci. Lett.*, 506, 520-529. <https://doi.org/10.1016/j.epsl.2018.11.020>.
- Reagan, M. K., et al. (2010), Fore-arc basalts and subduction initiation in the Izu-Bonin-Mariana system, *Geochem. Geophys. Geosyst.*, 11(3), doi:10.1029/2009GC002871.
- Schmeling, H., et al. (2008), A benchmark comparison of spontaneous subduction models—Towards a free surface, *Phys. Earth Planet. Inter.*, 171(1–4), 198-223, <http://dx.doi.org/10.1016/j.pepi.2008.06.028>.
- Shervais, J. W., M. Reagan, E. Haugen, R. R. Almeev, J. A. Pearce, J. Prytulak, J. G. Ryan, S. A. Whattam, M. Godard, and T. Chapman (2019), Magmatic response to subduction initiation: Part 1. Fore-arc basalts of the Izu-Bonin arc from IODP Expedition 352, *Geochem. Geophys. Geosyst.*, 20(1), 314-338. <https://doi.org/10.1029/2018GC007731>.
- Shuck, B., S. P. S. Gulick, H. J. A. Van Avendonk, M. Gurnis, R. Sutherland, J. Stock, and E. Hightower (2022), Stress transition from horizontal to vertical forces during subduction initiation, *Nat. Geosci.*, 15(2), 149-155, doi:10.1038/s41561-021-00880-4.
- Stern, R. J., and S. H. Bloomer (1992), Subduction zone infancy: examples

from the Eocene Izu-Bonin-Mariana and Jurassic California arcs, *Geol. Sco. Am. Bull.*, 104(12), 1621-1636.

Stern, R. J., and T. Gerya (2017), Subduction initiation in nature and models: A review, *Tectonophysics*, <https://doi.org/10.1016/j.tecto.2017.10.014>.

Sun, B., B. J. P. Kaus, J. Yang, G. Lu, X. Wang, K. Wang, and L. Zhao (2021), Subduction Polarity Reversal Triggered by Oceanic Plateau Accretion: Implications for Induced Subduction Initiation, *Geophys. Res. Lett.*, 48(24), e2021GL095299, <https://doi.org/10.1029/2021GL095299>.

Whattam, S. A., and R. J. Stern (2011), The ‘subduction initiation rule’: a key for linking ophiolites, intra-oceanic forearcs, and subduction initiation, *Contrib. Mineral. Petrol.*, 162(5), 1031-1045. <https://doi.org/10.1007/s00410-011-0638-z>.

Wolfson-Schwehr, M., and M. S. Boettcher (2019), Global characteristics of oceanic transform fault structure and seismicity, in *Transform plate boundaries and fracture zones*, edited, pp. 21-59, Elsevier.

Wolfson-Schwehr, M., M. S. Boettcher, J. J. McGuire, and J. A. Collins (2014), The relationship between seismicity and fault structure on the Discovery transform fault, East Pacific Rise, *Geochem. Geophys. Geosyst.*, 15(9), 3698-3712.

Wu, J., J. Suppe, R. Lu, and R. Kanda (2016), Philippine Sea and East Asian plate tectonics since 52 Ma constrained by new subducted slab reconstruction methods, *J. Geophys. Res.: Solid Earth*, 121(6), 4670-4741. <https://doi.org/10.1002/2016JB012923>.

Yang, J., and M. Faccenda (2020), Intraplate volcanism originating from upwelling hydrous mantle transition zone, *Nature*, doi:10.1038/s41586-020-2045-y.

Yang, J., G. Lu, T. Liu, Y. Li, K. Wang, X. Wang, B. Sun, M. Faccenda, and L. Zhao (2020), Amagmatic Subduction Produced by Mantle Serpentinization and Oceanic Crust Delamination, *Geophys. Res. Lett.*, 47(9), e2019GL086257, doi:10.1029/2019gl086257.

Zhong, X., and Z. H. Li (2019), Forced subduction initiation at passive continental margins: velocity-driven versus stress-driven, *Geophys. Res. Lett.* <https://doi.org/10.1029/2019GL084022>.

Zhou, X., Z.-H. Li, T. V. Gerya, R. J. Stern, Z. Xu, and J. Zhang (2018), Subduction initiation dynamics along a transform fault control trench curvature and ophiolite ages, *Geology*. <https://doi.org/10.1130/G40154.1>.

Zhou, X., and I. Wada (2021), Differentiating induced versus spontaneous subduction initiation using thermomechanical models and metamorphic soles, *Nat. Commun.*, 12(1), 4632, doi:10.1038/s41467-021-24896-x.

Supplementary references

Ranalli, G., 1995. *Rheology of the Earth*. Springer Science & Business Media.

Acknowledgments

This study is supported by the National Natural Science Foundation of China (Grants 41888101 and 41625016).

Data Availability Statement

The numerical code I2VIS used for numerical modeling (developed by T. Gerya) is freely available at <https://doi.org/10.17605/OSF.IO/bnvth>.

Figure captions

Fig. 1. Drilled rock types in Izu-Bonin-Mariana (IBM) and proposed subduction initiation. **(a)** The bathymetry in IBM. **(b)** The recovered rock sequence from the Bonin island (black star in a). **(c)** Horizontally forced subducting plate and sediment accretion at the trench, and **(d)** freely vertical plate sinking. Proposed SI and petrogenesis of forearc basalts (FAB), low-silica boninites (LSB), and high-silica boninites (HSB) are either horizontally forced or vertically forced. TF-transform fault, FZ-fracture zones.

Fig. 2. Initial model setup. The top 20 km is the viscous air layer (10^{18} Pa s); a certain width of the weak zone is set between a young and an old oceanic plate. The temperature contours are indicated with numbers in °C. All boundaries are free slip except the lower one which is permeable.

Fig. 3. Failed self-driven SI and forced SI. **(a)** Composition and **(b)** viscosity fields for no ignitor and failed SI, and **(c)** composition and **(d)** viscosity fields (superimposed with velocity field in arrows) for ignited and failed SI. **(e)** A summary of parameter regimes of SI for the width and viscosity of the transform fault/fracture zone. The gray contour lines in A-D are isotherms in °C.

Fig. 4. Petrogenesis evolution from subduction inception to mature. **(a)** Magmatic ignitor and cold slab sinking result in near trench seafloor spreading and early FAB, **(b)** extensive proto-forearc basalt formation and strongly depleted shallow mantle wedge alongside retreating slab, **(c)** pervasive slab dehydration and mantle/sediment melting, and **(d)** is the zoom out region of the box in **(c)**. The color legends for the composition are the same as in Fig. 2. The gray contours are isotherms in °C.

Fig. 5. Emergence of different volcanic/plutons along time. The extracted melting phases from **(a)** dry mantle and sediment and **(b)** wet mantle and basalt. Forearc basalt by dry mantle decompression melting, low-silica boninite by the involvement of slab melting, and high-silica boninite by flux-melting of the depleted residue of FAB.